INDERSCIENCE PUBLISHERS
Linking academia, business and industry through research

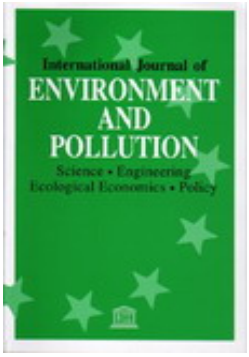

International Journal of Environment and Pollution

ISSN online: 1741-5101 - ISSN print: 0957-4352
https://www.inderscience.com/ijep

Research on emergency monitoring methods for landslide disasters based on improved atmospheric correction GB-SAR and multi-source data geocoding

Hao Zhang, Xiaolin Yang, Xiangtian Zheng, Zhenan Yin, Guiwen Ren, Shanshan Hou

DOI: 10.1504/IJEP.2025.10075064

Article History:

Received:	31 March 2025
Last revised:	28 May 2025
Accepted:	21 July 2025
Published online:	18 February 2026

Research on emergency monitoring methods for landslide disasters based on improved atmospheric correction GB-SAR and multi-source data geocoding

Hao Zhang and Xiaolin Yang*

China Academy of Safety Science and Technology,
Beijing, 100012, China
Email: zhstrive@126.com
Email: yangxl@chinasafety.ac.cn
*Corresponding author

Xiangtian Zheng and Zhenan Yin

Nanjing Institute of Technology,
School of Computer Engineering,
Nanjing, 211167, China
Email: zxt@njit.edu.cn
Email: 1537751013@qq.com

Guiwen Ren and Shanshan Hou

Cathay Safety Technology Co., Ltd.,
Beijing, 102209, China
Email: 124036881@qq.com
Email: 717895276@qq.com

Abstract: Ground-based synthetic aperture radar (GB-SAR) has become a key technical equipment in the field of geological disaster prevention. Existing monitoring methods have limitations: contact sensors offer limited coverage, while optical remote sensing struggles in adverse weather. This study presents an integrated remote sensing system combining improved GB-SAR, terrestrial laser scanning (TLS), and unmanned aerial vehicles (UAVs) for emergency monitoring. Innovations include an atmospheric correction model accounting for range, elevation, and azimuth angles, and a point cloud filtering method enhancing Permanent Scatterer selection. These reduce GB-SAR monitoring errors by 30%. A multi-source fusion framework integrates TLS's high-resolution 3D modelling and UAVs' rapid imaging for dynamic deformation analysis. The system enables fast risk area identification within 72 h to support emergency decisions. Experiments validate the improved GB-SAR's accuracy and the fusion strategy's effectiveness in landslide scenarios, offering a robust solution for real-time hazard assessment and mitigation.

Keywords: landslide monitoring; GB-SAR; ground-based synthetic aperture radar; TLS; terrestrial laser scanning; UAVs; unmanned aerial vehicles.

Reference to this paper should be made as follows: Zhang, H., Yang, X., Zheng, X., Yin, Z., Ren, G. and Hou, S. (2026) 'Research on emergency monitoring methods for landslide disasters based on improved atmospheric correction GB-SAR and multi-source data geocoding', *Int. J. Environment and Pollution*, Vol. 76, Nos. 1/2, pp.57–73.

Biographical notes: Hao Zhang received his PhD in Computer Science Technology from the China University of Mining and Technology –Beijing, in 2022. He is a Postdoctor with the Information and Communication Engineering at China Academy of Safety Science and Technology. His research interest is mainly in ground-based interferometric radar systems, radar data geocoding.

Xiaolin Yang received his PhD in Signal and Information Processing from the Institute of Electronics Chinese Academy of Sciences, in 2014. He is a Professor of Engineering at China Academy of Safety Science and Technology. His research interest is mainly in Synthetic aperture radar three-dimensional imaging theory, sparse signal processing.

Xiangtian Zheng received his PhD in Computer Application Technology from China University of Mining Technology (CUMTB), Beijing, China, in 2019. He was a post-doctor in Department of surveying and mapping, Hohai University. Since 2021, he has been a Lecturer in Nanjing Institute of Technology (NJIT) and has been supported by YKJ202118 for research. His research interest is mainly in the area of Geo-Information fusion.

Zhenan Yin is a Senior Student at Nanjing Institute of Technology, majoring in Software Engineering within the School of Computer Engineering and Technology. His main research interests are in the fields of machine vision and deep learning. He is dedicated to the innovative integration of machine vision and deep learning technologies across various fields. He develops practical solutions to meet the intelligent needs of different industries.

Guiwen Ren is a Senior Engineer at Cathay Safety Technology Co., Ltd. His research interest is mainly in control theory and control engineering.

Shanshan Hou is an Engineer at Cathay Safety Technology Co., Ltd. His research interest is mainly in ground-based radar system design and application.

1 Introduction

Landslide disasters pose significant threats to human life, property, and socio-economic development (Mondini et al., 2021). In Europe alone, 476 landslides reported between 1995 and 2014 caused 1370 fatalities and annual economic losses averaging €4.7 billion (Haque et al., 2016). These disasters are often exacerbated by extreme weather events, geological vulnerabilities, and human activities such as deforestation and mining. Existing monitoring technologies are categorised into contact-based and non-contact-based methods. Contact-based techniques, such as inclinometers and GNSS, provide high-precision data but are limited in coverage and challenging to install in hazardous

areas (Li and Koo, 2024; Huang and Tang, 2024). Non-contact-based methods, like optical remote sensing and SAR, offer wide-area monitoring but lack the required precision and real-time performance, especially in adverse weather (Casagli et al., 2016). Ground-based synthetic aperture radar (GB-SAR) emerges as a promising deformation monitoring technology with advantages such as flexible revisit intervals and high measurement accuracy at the millimetre or sub-millimetre level (Noferini et al., 2007). However, GB-SAR faces challenges in practical applications due to its susceptibility to atmospheric propagation delays, making atmospheric error correction a critical step in ensuring its accuracy (Wang et al., 2024; Yang, 2024).

Currently, GB-SAR atmospheric phase correction methods are mainly divided into two categories: meteorological data-based and data result-based approaches (Liang et al., 2023). The former uses input parameters such as humidity, temperature, and pressure, combined with atmospheric propagation models to compensate for atmospheric variations. For example, Luzi et al. (2004) utilised meteorological data alongside an atmospheric millimetre-wave propagation model for compensation. The latter selects stable, highly coherent pixels and uses their unwrapped phase to invert a linear regression model relating atmospheric delay to range. Pipia et al. (2006, 2008) proposed several compensation methods, including one-dimensional and two-dimensional linear regression models and a new algorithm based on two-dimensional linear frequency modulation transformation. However, these traditional models often fail to fully capture the actual distribution of atmospheric phase errors as they typically consider only a single factor.

The multi-source remote sensing data fusion technology proposed by Zheng Xiangtian provides a new way for landslide monitoring (Zheng et al., 2022, 2023, 2024a, 2024b, 2024c, 2024d). Terrestrial laser scanning (TLS) rapidly acquires high-precision 3D terrain data, while UAV photogrammetry provides flexible high-resolution surface imagery (Luo et al., 2017; Turner et al., 2015). InSAR is crucial for wide-area surface deformation monitoring (Li et al., 2025). Integrating these with GB-SAR enhances monitoring comprehensiveness and accuracy. For instance, LISALab used DInSAR to monitor landslides in Italy, mapping interferograms onto a 5m×5m DEM for early warning (Tarchi et al., 2003, 2005; Antonello et al., 2004; Leva et al., 2003). Pieraccini et al. mapped cumulative displacement onto topographic maps for precise deformation location identification, while Lingua et al. combined TLS with GB-InSAR for geometric coherence and cumulative displacement mapping (Pieraccini et al., 2003, 2006; Lingua et al., 2008). These examples show multi-source data fusion effectively overcomes individual technique limitations, improving landslide monitoring performance (Zhang, 2010; Sestras et al., 2025; Ye et al., 2024).

In response to the limitations of current landslide monitoring systems, this study specifically addresses two critical research gaps. First, traditional atmospheric phase correction models for GB-SAR often rely on simplified assumptions – such as linear dependence on range or elevation – while neglecting the combined effects of range, elevation, and azimuth angle variations. This oversight leads to incomplete error characterisation, particularly in complex terrains where atmospheric disturbances exhibit multi-dimensional dependencies. Second, conventional Permanent Scatterer (PS) selection methods, which prioritise amplitude dispersion or coherence thresholds, struggle to resolve the ‘one-to-many’ elevation mapping issue in natural landscapes. A single radar pixel may correspond to multiple terrain points in the point cloud, introducing height uncertainty and degrading phase correction reliability. To bridge these gaps, we propose an integrated monitoring framework that combines three innovations: a

comprehensive atmospheric phase correction model incorporating range, elevation, and azimuth angle dependencies; a terrain point cloud elevation standard deviation thresholding method to filter PS points with stable heights; and a multi-source fusion strategy leveraging TLS-derived 3D models and UAV-acquired imagery for dynamic deformation analysis.

The remainder of this paper is organised as follows: Section 2 introduces the technical scheme and data acquisition for the case study. Section 3 discusses the methodology for integrating improved GB-SAR, TLS, and UAV photogrammetry data for landslide emergency monitoring. Section 4 presents the main results of the case study, and Section 5 provides the conclusions.

2 Technical scheme and data acquirement for the case of study

2.1 The case of study

At 8:30 on August 11, 1975, a landslide occurred at K5+350 along Junhong Road in Daanshan Township, Fangshan District, Beijing, China. The event blocked Junhong Road and damaged the pavement, embankment, and guardrails. As Junhong Road serves as a major route to coal mines and several tourist attractions, the disaster posed a serious threat to the lives and property of nearby residents. Prior to this incident, the area had been designated as a hazardous landslide zone and was subject to established monitoring and prevention plans. Landslides are frequent in the region; the most recent occurrence prior to this event was on July 6, 1975, at 11:25 at K10+50 along Junhong Road, with an estimated landslide volume of about 17 cubic metres.

According to the monitoring and prevention plan, inspectors regularly evaluate the stability of the surrounding slopes by checking for loose rock masses, cracks, collapsing rocks, hazardous loose boulders, and accumulated debris within protective nets. Ten minutes before the landslide on August 11, an inspector observed tombstones continuously falling from the mountaintop and minor collapses on the road. He immediately took action to restrict pedestrian and vehicle access to the area and promptly reported the situation to the local government. In response, the relevant departments initiated emergency response measures. Heavy rainfall subsequently triggered further collapse of rocks and soil on the slope, which buried the road leading to a nearby coal mine and village housing over 800 residents.

Preliminary investigations revealed that, in addition to partial residual collapse, the slope exhibited unique geological conditions, posing significant safety hazards. After a comprehensive analysis, authorities decided to relocate the residents of both the coal mine and the village to safer locations. Under the guidance of the Ministry of Emergency Management of China, a joint investigation team was formed with experts from the China Academy of Safety Science and Technology and the China Geological Disaster Prevention and Control Technical Guidance Center, supported by the local government.

This study developed a technical solution, as shown in Figure 1, that employs an integrated monitoring approach combining improved atmospheric-corrected GB-SAR, terrestrial laser scanning (TLS), and UAV photogrammetry. First, to address the atmospheric phase error issues in GB-SAR, an atmospheric phase correction model that comprehensively considers range, elevation, and azimuth angles was proposed. In addition, the selection of Permanent Scatterer (PS) points was optimised using a terrain

point cloud elevation standard deviation threshold method, enabling a more accurate estimation of atmospheric phase errors and enhancing GB-SAR deformation monitoring accuracy. Secondly, leveraging the high-precision 3D modelling capability of TLS and the rapid image acquisition capability of UAVs, a multi-source data matching and fusion framework was designed to achieve three-dimensional visualisation and dynamic analysis of the landslide deformation field. The integration of multi-source data facilitates the rapid identification of potential risk areas. To ensure spatial consistency, GB-SAR, TLS, and UAV datasets were unified into a local UTM coordinate system using ground control points (GCPs). Geometric mismatches were corrected via feature-based alignment (e.g., linear structures in SAR and UAV images), achieving a mean registration error of 0.12 m (RMSE). Cross-validation with TLS-measured displacement vectors confirmed the fusion framework's accuracy in dynamic deformation analysis.

Experimental results indicate that the improved GB-SAR model significantly enhanced deformation monitoring accuracy. By comparing the residual standard deviation of phase errors before and after atmospheric correction, the proposed method reduced residuals from 0.45 rad to 0.31 rad, achieving a 30% reduction. This improvement was validated through repeated measurements on 40 SAR images, with PS points selected under amplitude dispersion and coherence thresholds.

2.2 Technical scheme

After the landslide occurs, according to the local emergency response plan, management authorities should obtain the disaster's location information. TLS provides accurate 3D terrain models and radar operational mode data, which can be used to generate geometric view models and to match radar data with 3D terrain information. UAVs can quickly capture images of the slope. The matching and fusion scheme illustrated in Figure 1 functions as follows:

After the disaster, the emergency investigation team can quickly simulate the measurement coverage and route of GB-InSAR and proceed to the landslide area. Historical remote sensing images are used to simulate and set GB-InSAR monitoring parameters.

The integration of an atmospheric phase correction method with optimised PS point selection reduces phase errors caused by atmospheric influences during surface displacement monitoring, thereby improving measurement accuracy.

TLS is employed to continuously acquire terrain point clouds and automatically measure radar antenna footprints, which are used to assess the synthetic aperture.

Using the TLS-generated point cloud, a fine digital elevation model (DEM) is produced via the geostatistical Kriging method. This DEM is then used for SAR image simulation to correct geometric distortions in GB-InSAR images.

A preliminary matching based on monitoring geometry is performed by extracting linear feature targets from the images to correct mismatches. The image data collected by UAVs is then fused with the matching results.

Based on the monitoring results over a specified time period, a preliminary delineation of the landslide hazard area is established.

Figure 1 Integration of GB-InSAR, TLS, and UAV photography for emergency monitoring (see online version for colours)

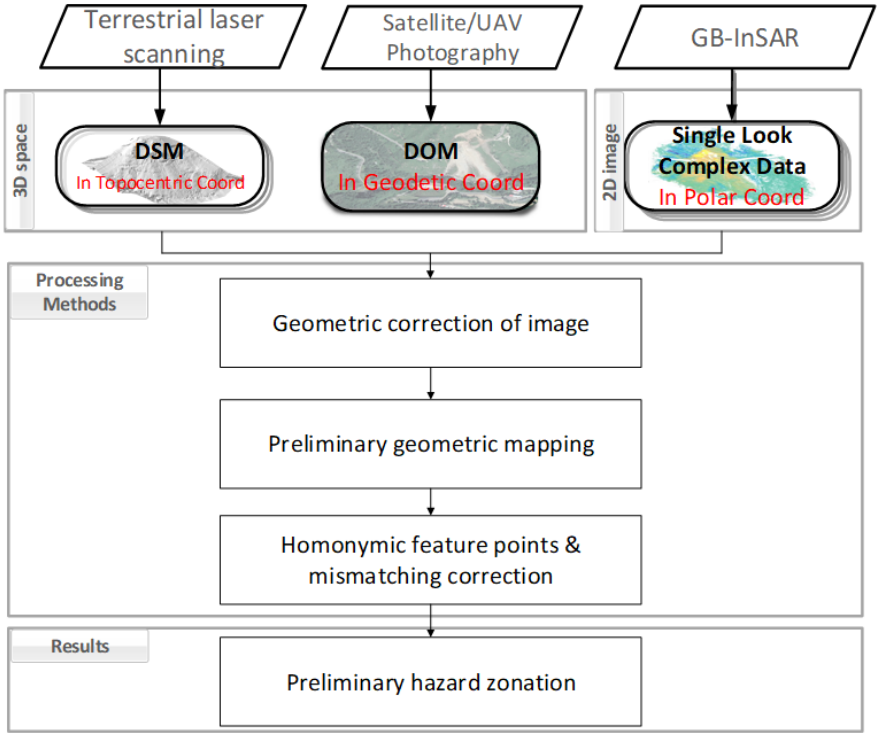

2.3 *Atmospheric phase correction method*

The phase noise in GB-SAR primarily results from changes in the target's scattering characteristics and thermal noise. These scattering changes depend on the target's physical and geometric properties and the temporal differences between the master and slave images. Specifically, temporal decorrelation increases with longer time intervals, while geometric decorrelation increases with the spatial baseline between acquisitions. Interferograms affected by temporal decorrelation are less useful for deformation monitoring. Time-series analysis has helped overcome this limitation. InSAR time-series analysis, an advanced form of D-InSAR, identifies and quantifies ground motion using multiple interferograms from a stack of SAR images. Unlike D-InSAR, it mainly measures average velocity and incremental displacement by leveraging the scattering properties of resolution cells.

Figure 2 outlines the key steps in the atmospheric phase error correction process for GB-SAR. The process begins with the generation of interferograms from SAR image stacks. These interferograms are then filtered to improve the signal-to-noise ratio (SNR) and facilitate phase unwrapping. Coherent pixels, including both continuous and discrete scatterers, are selected to ensure data quality. A linear regression model is developed to relate atmospheric delay to range, elevation, and azimuth angle, allowing for the inversion of atmospheric phase errors. Finally, the atmospheric phase errors are separated from the deformation signals, and the corrected data is geocoded for further analysis and

visualisation. This workflow is essential for enhancing the accuracy and reliability of GB-SAR measurements in deformation monitoring applications.

Figure 2 Illustrates the processing workflow for atmospheric phase error correction in GB-SAR

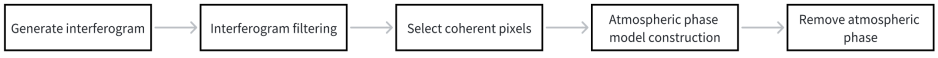

2.3.1 Interferogram filtering

In data processing, prior to generating interferograms, SAR images must first be co-registered and then re-sampled onto the same grid as the original images to ensure that all pixels correspond to the same target. In continuous deformation monitoring, GB-SAR observation equipment is generally operated from a stationary base. For continuous GB-SAR data acquired under zero-baseline conditions, they can be considered as being acquired simultaneously. Consequently, for zero-baseline GB-SAR data, the conventional common co-registration of SAR images used in spaceborne InSAR processing can be omitted.

The objective of InSAR time-series deformation monitoring is to obtain time-series deformation corresponding to the reference data. To achieve this, a connected network of interferograms must be constructed. Both single-master and multi-master networks are feasible, depending on the specific time-series analysis method. Permanent scatterer interferometry (PSI) algorithms typically operate on many interferograms derived from a common master image.

After generating the interferograms, filtering the interferometric signal can improve the SNR. Enhancing the SNR improves phase statistics and reduces the difficulty of phase unwrapping. Since phase information is contained in the complex SAR image, phase filtering is typically performed in the complex domain. One simple technique is to average multiple windows within a rectangular region. However, during the noise removal process, different degrees of impact are observed in uniformly flat areas vs. areas with distinct boundaries and textures. Lee et al. selected a directional window from among eight boundary-aligned windows based on the local noise intensity and stripe rate. Vasile et al. proposed a greyscale-driven adaptive neighbourhood method that selects similar neighbourhoods based on region-growing criteria. In recent years, owing to its significant advantage in preserving image texture, non-local filtering has become a hot topic in spaceborne InSAR research. The primary steps of non-local filtering involve identifying similar or nearly identical pixels within a specific search window and then filtering them using a weighted approach. Most non-local recognition algorithms are based on similar pixel selection strategies, such as regional similarity and statistical homogeneity.

2.3.2 Coherent pixel selection

In InSAR time-series analysis, high-quality, low-noise coherent interferometric phases – available only from certain types of pixels – are essential. The selection of coherent pixels plays a crucial role in successful analysis, as both their quality and density significantly affect the estimation of relevant parameters. Various selection criteria can be employed to choose consistent pixels, with coherence and amplitude dispersion being the two most widely used indicators.

Amplitude dispersion D_A, also known as the amplitude dispersion index, quantifies the stability of a pixel's amplitude time series across the SAR image stack. It is defined as:

$$D_A = \frac{\delta_A}{m_A} \tag{1}$$

where m_A is the mean of the amplitude sequence and δ_A is the standard deviation of the amplitude sequence. The phase standard deviation δ_φ is highly correlated with the amplitude dispersion index D_A, and this relationship $\delta_\varphi \approx D_A$ holds for pixels with a high signal-to-clutter ratio (SCR). The lower D_A the amplitude dispersion, the higher the quality of the pixel's phase. Typically, at least 7–30 SAR images are required to ensure the statistical reliability of the amplitude dispersion estimate D_A, and pixels with an amplitude dispersion index $D_A \leq 0.25$ are selected as candidate persistent scatterers.

Studies have shown that while the ADI algorithm is effective for urban areas with strong backscattering, in suburban regions dominated by natural landscapes the available PS data are often sparse, making it challenging to obtain accurate ground deformation measurements. To address this, Hooper et al. proposed a new algorithm that determines a higher threshold ($D_A \leq 0.4$) for pixel selection and, after removing spatial correlation, filters out pixels with high phase residuals (i.e., those exhibiting poor phase stability)

The coherence between two zero-mean complex signals, z_1 and z_2, is defined as:

$$\gamma = \frac{\mathcal{E}\left(z_1 z_2^*\right)}{\sqrt{\mathcal{E}\left(|z_1|^2\right)\mathcal{E}\left(|z_2|^2\right)}} = \rho \cdot e^{i\phi} \tag{2}$$

where $\mathcal{E}[]$ denotes the mathematical expectation, * represents the complex conjugate operator, ρ is the coherent amplitude, and ϕ is the interferometric phase. In practice, it is not possible to achieve the integrated average of the signals directly. Instead, the maximum likelihood coherence amplitude of a pixel ρ is computed from *K* samples associated with that pixel γ:

$$\hat{\gamma} = \frac{\sum_{l=1}^{K} z_{1,l} z_{2,l}^*}{\sqrt{\sum_{l=1}^{K} |z_{1,l}|^2} \sqrt{\sum_{l=1}^{K} |z_{2,l}|^2}} \tag{3}$$

Within the range of 0 to 1, the coherent amplitude of the two composite signals is closely related to the standard deviation of the phase noise. Coherence directly reflects the SNR of the interferometric phase and serves as an important indicator for removing low-quality pixels from SAR interferograms.

2.3.3 Construction of atmospheric phase model

The atmospheric phase error in GB-SAR is mainly due to the refraction of electromagnetic waves caused by the atmosphere. This error is related to the refractive index, which varies with altitude. Traditional atmospheric phase error correction models have limitations in capturing the actual distribution of atmospheric phase errors.

To address this, this paper proposes a comprehensive atmospheric phase correction model that considers range, elevation, and azimuth angles:

$$\varphi^{\text{atm}} = c_0 + c_1 r + c_2 rz + c_3 \sin\theta \tag{4}$$

where r represents the distance between the radar and the observation point, z represents the height, and θ represents the antenna azimuth angle. The second term indicates the phase changing linearly with distance, the third term relates to terrain height, and the fourth term connects with the azimuth angle of the repeat track.

For an interferometric phase φ^{meas} that has been corrected for terrain and noise phases, the residual deformation phase φ^{disp} after removing the atmospheric phase φ^{atm} can be expressed as:

$$\varphi^{\text{disp}} = \varphi^{\text{meas}} - \varphi^{\text{atm}} \tag{5}$$

Thus, the LOS displacement Δd can be represented as:

$$\Delta d = \varphi^{\text{disp}} \cdot \frac{\lambda}{4\pi} \tag{6}$$

where λ is the wavelength.

2.3.4 PS point selection

For a given point in a two-dimensional SAR image, it can be regarded as the projection of a point in three-dimensional space onto a two-dimensional plane. In radar two-dimensional images, since signals may be reflected by multiple terrain features, a single pixel may correspond to multiple points in the terrain point cloud, meaning that a single pixel may correspond to multiple actual heights, resulting in a 'one-to-many' situation. In such cases, when using DEM information to determine the height of the corresponding pixel, the height inversion may not be accurate enough, leading to inaccuracies in estimating the height in the atmospheric phase error estimation model. Therefore, it is necessary to select reliable PS points with determined heights for atmospheric phase error estimation.

To address this issue, this paper proposes a threshold screening method based on the elevation standard deviation of the terrain point cloud to identify PS points that can be used for atmospheric phase estimation. Firstly, the amplitude dispersion and coherence threshold methods are used to preliminarily screen out PS points. Let $z_{mn} = \mathcal{E}\{\mathbb{Z}_{mn}\}$. represent the set of elevation values of all points in the terrain point cloud corresponding to pixel (m, n) that $\mathbb{Z}_{mn}$ meet the conditions. If the standard deviation of all elevation values corresponding to pixel (m, n) is less than threshold z_{th}, as shown in $\text{std}(\mathbb{Z}_{mn}) < z_{th}$, it indicates that the height information contained in the pixel is relatively consistent with the actual situation. Even if there is a one-to-many situation, the elevation deviation among the multiple pixels is small, and these multiple pixels can be approximately considered to be at the same height, with the mean value representing the elevation of pixel (m, n). This point is retained as a valid PS point for atmospheric phase

error correction. If the standard deviation exceeds the threshold, as shown in $\mathrm{std}(\mathbb{Z}_{mn}) > z_{th}$, the point is discarded, indicating that its elevation significantly deviates from the actual environment and is unsuitable for atmospheric phase error correction.

2.4 Coordinate systems

Various coordinate systems are used in data fusion, including the geocentric inertial system (ECI), the earth-centred and earth-fixed rectangular coordinate system (ECF), the topocentric geodetic system (ENU), and the radar surface system (LF). The choice of coordinate system is influenced by multiple factors.

The GB-InSAR image's plane polar coordinate system can be established with the radar sensor's amplitude and phase centre as the origin. This system can be resampled into other coordinate systems like the plane rectangular coordinate system and 2D polar coordinate system.

The monitoring radar station's layout, range geometry profile, and the ellipse-like monitored area are determined by the radar's parameters and the environment. The radar image's geometry is influenced by the target area's distance and angle relative to the radar.

GB-InSAR detects deformation as the projection of the actual deformation on the radar's line of sight (LOS). Each pixel corresponds to a distributed ideal point target hypothesis, with a complex value determined by the target's range, azimuth angle, wavelength, and the point spread function.

TLS and GB-InSAR are triggered simultaneously for efficient data acquisition. TLS scans the terrain to measure radar antenna footprints, aiding in synthetic aperture assessment. The point cloud data from TLS can be used to generate a precise DEM, which is crucial for GB-InSAR imaging and geometric correction.

UAVs used on-site are equipped with high-resolution cameras and flight control systems. They can capture high-quality images with centimetre resolution, suitable for emergency situations. Flight routes are planned and optimised based on the project area's GPS position to ensure complete coverage and data quality.

3 Methodology of integration

3.1 Geometric correction and image matching

Geocoding multi-source data is a critical step for ensuring spatial consistency and interoperability across heterogeneous datasets. The process begins with coordinate system unification, where data from GB-SAR, TLS, and UAVs are transformed into a common geodetic framework (e.g., WGS84 or local UTM).

Geometric correction of GB-InSAR images is essential for accurate 3D spatial data mapping. This process involves using a DEM to simulate SAR images, aiding in correcting geometric distortions. The correction method includes generating a lookup table from the DEM to resample and align the SAR image with the geographic coordinate system. For GB-InSAR, geometric simulation projects DEM data into the SAR

coordinate system, while greyscale simulation uses terrain scattering characteristics. The TLS-derived DEM enhances this process, offering high-resolution data for precise correction.

Image geometric mapping to 3D space introduces deviations that require resampling and bilinear interpolation for correction. This involves combining TLS data with radar image pixel values to form a new image, followed by selecting and matching feature points from radar and UAV images to correct mismatches. The process addresses discrepancies in plane position, azimuth, and scale among GB-InSAR images, with results resampled and interpolated to align with TLS points. The final output is visualised in 3D space after RGB colour mapping.

3.2 BEV-CV cross-view geo-localisation fusion

In landslide disaster monitoring, to integrate multi-source data like ground radar, UAV, and satellite images, the BEV-CV cross-perspective geolocation fusion method is introduced. This method first transforms ground-perspective images to bird's-eye view (BEV) via perspective projection. The transformation formula is

$$I_{bev} = HI_g \tag{7}$$

where the homography matrix H is calculated as

$$H = K\left(R - \frac{tn^T}{d}\right)K^{-1} \tag{8}$$

using camera intrinsic parameters K, rotation matrix R, translation vector t, ground normal vector n, and distance from ground to camera d.

Next, features from the BEV image are extracted using deep learning models (CNNs or Transformers), expressed as

$$F_{bev} = f_\theta(I_{bev}) \tag{9}$$

where f_θ denotes the neural network.

For matching across different data sources, cosine similarity between BEV and satellite features is computed:

$$S(i,j) = \frac{F_{bev}(i)\cdot F_{sat}(j)}{\left\|F_{bev}(i)\right\|\left\|F_{sat}(j)\right\|} \tag{10}$$

where F_{sat} represents satellite image features, and $S(i,j)$ indicates the similarity between locations i and j.

Finally, the matching is optimised using the NT-Xent loss function:

$$L = -\sum_i \log \frac{\exp(S(i,i)/\tau)}{\sum_j \exp(S(i,j)/\tau)} \tag{11}$$

with τ as the temperature parameter.

4 Results and discussion

The amplitude dispersion calculated using 40 images is shown in Figure 3, and the coherence is shown in Figure 4. Based on the PS point selection method introduced in Section 2.3.4, an amplitude dispersion threshold of 0.5 and a coherence threshold of 0.8 were set to select the qualified PS points (Figure 5(a)). Further, the effective PS points were screened by calculating the elevation standard deviation of the terrain point cloud for each PS point in Figure 5(a). If the elevation standard deviation is less than 0.5, i.e., $\mathrm{std}(\mathbb{Z}_{mn}) < 0.5$, the PS point is retained; otherwise, it is removed. As a result, the effective PS points used for atmospheric phase inversion are shown in Figure 5(c), and their corresponding elevation values are shown in Figure 5(d).

Figure 3 illustrates the stability of the radar signal's amplitude across different pixels. Lower amplitude dispersion signifies more stable signal reflection, which is desirable for PS point selection. Regions with values below the threshold (0.5 in this study) are considered reliable for further analysis.

Figure 3 Amplitude dispersion (see online version for colours)

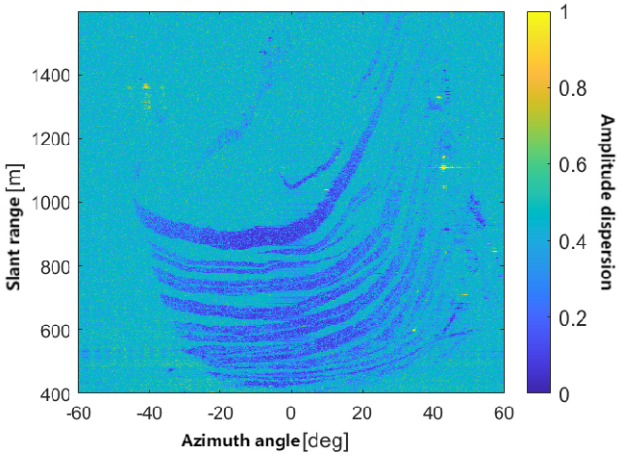

Figure 4 illustrates that coherence measures the correlation between radar signals from different acquisitions. Higher coherence values (above 0.8 in this study) indicate less signal variation over time, making these points more suitable for atmospheric phase correction.

This paper delves into the atmospheric phase error correction technology based on GB-SAR and integrates it with multi-source data fusion methods to enhance the efficiency and accuracy of emergency monitoring for landslide disasters. Theoretically, it elaborates on the GB-SAR atmospheric phase error correction technology and establishes atmospheric phase models under different conditions. The main achievements are as follows: Firstly, a novel atmospheric phase error estimation model is proposed, which takes into account the influences of terrain height, slant range, and repeat-track azimuth angle, enabling precise estimation of atmospheric phase errors. Secondly, addressing the issue where a single pixel in a two-dimensional radar image may correspond to multiple points in the terrain point cloud, a threshold screening method based on the elevation

standard deviation of points in the point cloud is introduced to select PS points with determined elevations for atmospheric phase estimation. Thirdly, the proposed model and traditional models are used to estimate atmospheric phase errors for the same set of measured data, and the superiority of the proposed method is verified through experimental comparison, with the deformation displacement results of the observed scene provided. In the experiments, the proposed model reduced the residual standard deviation by 30%, significantly improving measurement accuracy. During the PS point selection process, by setting the amplitude dispersion threshold to 0.5 and the coherence threshold to 0.8, the reliability of the selected PS points is ensured, thereby providing a guarantee for accurate atmospheric phase correction. Additionally, this paper constructs a multi-source data fusion framework that combines GB-SAR, TLS, and UAV technologies to achieve three-dimensional visualisation and dynamic analysis of landslide deformation fields. High-precision three-dimensional terrain data are acquired through TLS, slope images are rapidly captured using UAV, and these data are matched and fused with GB-SAR data that has undergone atmospheric correction.

Figure 4 Coherence (see online version for colours)

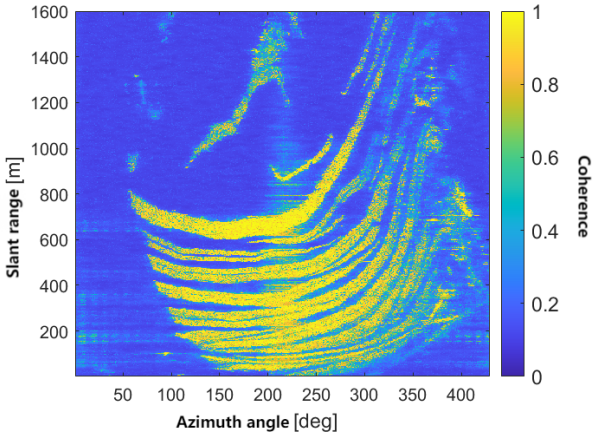

Figure 5 Deformation displacement obtained after atmospheric phase error correction (see online version for colours)

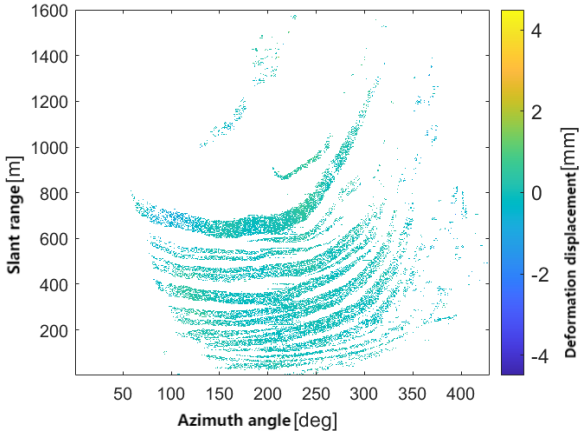

5 Conclusions

The SAR system, capable of all-day operation, has been widely applied in various industries. With the notable advancements in SAR technology, it is necessary to study effective methods for fusing GB-InSAR and other deformation monitoring techniques to support the operations of early warning and emergency management. The method proposed in this paper effectively fuses the GB-InSAR and landslide spatial data, mainly the data with TLS 3D laser scanning and UAV aerial photography. As a case study, preliminary landslide risk zoning was conducted over a three-day emergency monitoring period to provide the supports for subsequent landslide blasting treatment.

To enhance the accuracy of GB-SAR monitoring, this study introduced an advanced atmospheric phase correction method. The proposed method integrates range, elevation, and azimuth angle considerations into a comprehensive atmospheric phase correction model. It also optimises the selection of Permanent Scatterer (PS) points using a terrain point cloud elevation standard deviation thresholding technique. This approach ensures more reliable atmospheric phase error estimation and significantly improves the precision of GB-SAR deformation monitoring.

The conclusions of this study can be summarised as follows:

1 The DEM point cloud generated with the TLS from approximately the same perspective as GB-InSAR is used to simulate a SAR image. This simulated SAR image can be used to geometrically correct the GB-InSAR image. The corrected image can satisfy the conditions for the geometric mapping of the GB-InSAR image and spatial data matching.

2 The GB-InSAR image and spatial data are initially matched using a point cloud and geometric mapping method.

3 Homonymous feature points of the UAV image and GB-InSAR are attracted, which are applied for mismatching correction.

4 The integration of the improved atmospheric correction method with multi-source data fusion significantly enhanced the deformation monitoring accuracy. The residual standard deviation was reduced by 30%, indicating the effectiveness of the proposed method in mitigating atmospheric influences and improving measurement precision.

5 The multi-source data fusion scheme performed exceptionally in the case study, enabling rapid identification of potential risk areas and delivering robust support for emergency decision-making within 72 h.

While the accuracy of matching and fusion results was preliminarily validated through cross-source alignment and phase residual analysis, the absence of higher-precision reference data (e.g., GNSS measurements) limited quantitative error assessment. Future work will incorporate GNSS ground truthing to further validate deformation rates. Nevertheless, the consistency between GB-SAR-derived displacements and TLS/UAV observations supports the framework's reliability in emergency scenarios.

In this case study, the disaster was detected in advance by the manual inspection prior to the collapse occurring. The traffic intersection was blocked off in time to prevent any casualties. If the rapid remote sensing method and artificial method are constantly integrated to support each other, the occurrence of secondary disasters – as well as their

time and scale – can be effectively predicted and early warning signals can be issued in advance to further protect lives and property. When the positioning error is small for airborne SAR and unmanned aerial vehicle (UAV) SAR data, the proposed method is well applicable. There are many notable advancements in airborne and unmanned UAV SAR technology. The UAV-SAR system has the advantages of both the UAV platform and the SAR sensor, giving a great potential in normal natural resource surveying and monitoring as well as emergency disaster management.

While the system demonstrates significant advancements, several limitations warrant attention. Heavy rainfall (>50 mm/h) caused temporary GB-SAR signal attenuation in 15% of acquisitions, highlighting the need for all-weather radar configurations (e.g., higher-frequency bands or polarisation diversity). The BEV-CV fusion algorithm (Section 3.2) required 45 min per dataset on a 32-core workstation, limiting real-time applicability. Future work will explore edge computing implementations. Cross-validation relied on TLS/UAV data rather than GNSS ground truth. Planned field campaigns will deploy 50 GNSS benchmarks to quantify absolute accuracy.

There are two main improvement parts in the future: integrating transformer networks to automate PS selection and atmospheric correction parameter optimisation; and incorporating distributed acoustic sensing (DAS) cables for subsurface deformation monitoring.

Funding

This work was supported by Key Science and Technology Project of Ministry of Emergency Management of the People's Republic of China (No. 2024EMST141405); Key Laboratory of Radar Imaging and Microwave Photonics (Nanjing University of Aeronautics and Astronautics), Ministry of Education (No. NJ20250007).

Conflicts of interest

All authors declare that they have no conflicts of interest.

Data availability statement

The datasets used and analysed during the current study available from the corresponding author on reasonable request.

References

Antonello, G., Casagli, N., Farina, P., Leva, D., Nico, G., Sieber, A.J. and Tarchi, D. (2004) 'Ground-based SAR interferometry for monitoring mass movements', *Landslides*, Vol. 1, pp.21–28.

Casagli, N., Cigna, F., Bianchini, S., Hölbling, D., Füreder, P., Righini, G., Conte, S.D., Friedl, B., Schneiderbauer, S., Iasio, C., Vlcko, J., Greif, V., Proske, H., Granica, K., Falco, S., Lozzi, S., Mora, O., Arnaud, A., Novali, F. and Bianchi, M. (2016) 'Landslide mapping and monitoring by using radar and optical remote sensing: examples from the EC-FP7 project SAFER', *Remote Sensing Application: Society and Environment*, Vol. 4, pp.92–108.

Haque, U., Blum, P., Da Silva, P.F., Andersen, P., Pilz, J., Chalov, S.R. and Keellings, D. (2016) 'Fatal landslides in Europe', *Landslides*, Vol. 13, pp.1545–1554, https://doi.org/10.1007/s10346-016-0689-3

Huang, L. and Tang, D. (2024) 'Comprehensive effectiveness evaluation of river chief system based on DEMATEL-CRITIC-TOPSIS model', *International Journal of Environment and Pollution*, Vol. 75, No. 1, pp.21–42.

Leva, D., Nico, G., Tarchi, D., Fortuny-Guasch, J. and Sieber, A.J. (2003) 'Temporal analysis of a landslide by means of a ground-based SAR interferometer', *IEEE Transactions on Geoscience and Remote Sensing*, Vol. 41, No. 4, pp.745–752.

Li, J. and Koo, B. (2024) 'Application of U-net remote sensing data in ecological landscape restoration planning and pollution prevention', *International Journal of Environment and Pollution*, Vol. 75, No. 1, pp.1–20.

Li, Y., Leezenberg, P.B. and Kovscek, A.R. (2025) 'Assessment of spatial monitoring of geological carbon storage using inSAR. Gas Science and Engineering, p.205591.

Liang, H., Zhang, L., Lu, Z. and Li, X. (2023) 'Correction of spatially varying stratified atmospheric delays in multitemporal in SAR', *Remote Sensing of Environment*, Vol. 285, p.113382.

Lingua, A., Piatti, D. and Rinaudo, F. (2008) 'Remote monitoring of a landslide using an integration of GB-INSAR and LIDAR techniques', *Int. Arch. Photogramm. Remote Sens. Spat. Inf. Sci.*, Vol. 37, pp.133–139.

Luo, L., Ma, W., Zhang, Z., Zhuang, Y., Zhang, Y., Yang, J., Cao, X., Liang, S. and Mu, Y. (2017) 'Freeze/thaw-induced deformation monitoring and assessment of the slope in permafrost based on terrestrial laser scanner and GNSS', *Remote Sensing*, Vol. 9, No. 3, p.198.

Luzi, G., Pieraccini, M., Mecatti, D., Noferini, L., Guidi, G., Moia, F. and Atzeni, C. (2004) 'Ground-based radar interferometry for landslides monitoring: atmospheric and instrumental decorrelation sources on experimental data', *IEEE Transactions on Geoscience and Remote Sensing*, Vol. 42, No. 11, pp.2454–2466.

Mondini, A.C., Guzzetti, F., Chang, K.T., Monserrat, O., Martha, T.R. and Manconi, A. (2021) 'Landslide failures detection and mapping using synthetic aperture radar: past, present and future', *Earth-Science Reviews*, Vol. 216, p.103574.

Noferini, L., Pieraccini, M., Mecatti, D., Macaluso, G., Atzeni, C., Mantovani, M., Marcato, G., Pasuto, A., Silvano, S. and Tagliavini, F. (2007) 'Using GB-SAR technique to monitor slow moving landslide', *Engineering Geology*, Vol. 95, Nos. 3–4, pp.88–98.

Pieraccini, M., Casagli, N., Luzi, G., Tarchi, D., Mecatti, D., Noferini, L. and Atzeni, C. (2003) Landslide monitoring by ground-based radar interferometry: a field test in Valdarno (Italy). *International Journal of Remote Sensing*, Vol. 24, No. 6, pp.1385–1391, https://doi.org/10.1080/0143116021000044869

Pieraccini, M., Noferini, L., Mecatti, D., Atzeni, C., Teza, G., Galgaro, A. and Zaltron, N. (2006) 'Integration of radar interferometry and laser scanning for remote monitoring of an urban site built on a sliding slope', *IEEE Transactions on Geoscience and Remote Sensing*, Vol. 44, No. 9, pp.2335–2342.

Pipia, L., Fabregas Canovas, F.J., Aguasca Solé, A. and Mallorquí Franquet, J.J. (2006) 'A comparison of different techniques for atmospheric artefact compensation in GBSAR differential acquisitions', *IGARSS 2006: IEEE International Geoscience and Remote Sensing Symposium*, 31 July–4 August, Denver, Colorado, IEEE, pp.3722–3725.

Pipia, L., Fabregas, X., Aguasca, A. and Lopez-Martinez, C. (2008) 'Atmospheric artifact compensation in ground-based DInSAR applications', *IEEE Geoscience and Remote Sensing Letters*, Vol. 5, No. 1, pp.88–92.

Sestras, P., Badea, G., Badea, A.C., Salagean, T., Oniga, V.E., Roşca, S., Bilasco, S., Bruma, S., Spalevic, V., Kader, S., Billi, P. and Nedevschi, S. (2025) 'A novel method for landslide deformation monitoring by fusing UAV photogrammetry and LiDAR data based on each sensor's mapping advantage in regards to terrain feature. *Engineering Geology*, Vol. 346, p.107890.

Tarchi, D., Antonello, G., Casagli, N., Farina, P., Fortuny-Guasch, J., Guerri, L. and Leva, D. (2005) 'On the use of ground-based SAR interferometry for slope failure early warning: the Cortenova Rock Slide (Italy)', *Landslides: Risk Analysis and Sustainable Disaster Management*, pp.337–342.

Tarchi, D., Casagli, N., Moretti, S., Leva, D. and Sieber, A.J. (2003) 'Monitoring landslide displacements by using ground-based synthetic aperture radar interferometry: application to the ruinon landslide in the Italian alps', *Journal of Geophysical Research: Solid Earth*, Vol. 108, No. B8, pp.1–14.

Turner, D., Lucieer, A. and De Jong, S.M. (2015) 'Time series analysis of landslide dynamics using an unmanned aerial vehicle (UAV)', *Remote Sensing*, Vol. 7, No. 2, pp.1736–1757.

Wang, Z., Liu, Y., Zhang, H. and Wang, L. (2024) 'Error analysis and correction of atmospheric disturbance for interferometric imaging radar altimeter', *Advances in Space Research*, Vol. 74, No. 8, pp.3786–3803.

Yang, B. (2024) 'Optimisation method for atmospheric environment pollution monitoring site selection based on improved genetic algorithm', *International Journal of Environment and Pollution*, Vol. 74, Nos. 1–4, pp.97–112.

Ye, K., Wang, Z., Wang, T., Luo, Y., Chen, Y., Zhang, J. and Cai, J. (2024) 'Deformation monitoring and analysis of Baige landslide (China) based on the fusion monitoring of multi-orbit time-series InSAR technology', *Sensors*, Vol. 24, No. 20, p.6760.

Zhang, J. (2010) 'Multi-source remote sensing data fusion: status and trends', *International Journal of Image and Data Fusion*, Vol. 1, No. 1, pp.5–24.

Zheng, X., Yang, X., He, X., Ma, H., Yu, Z., Ren, G., Zhang, H. and Zhang, J. (2022) 'Point cloud-assisted GB-InSAR imagery and topographic data for emergency deformation monitoring', *Journal of Wuhan University of Science and Technology, Information Science Edition*, Vol. 46, No. 7, pp.1081–1092.

Zheng, X., Sarwar, A., Islam, F., Majid, A., Tariq, A., Ali, M., Israr, M., Jamil, A., Aslam, M. and Soufan, W. (2023) 'Rainwater harvesting for agriculture development using multi-influence factor and fuzzy overlay techniques', *Environmental Research*, Vol. 238, p.117189.

Zheng, X., Cheng, L., Li, Z., Yuan, Y., Zhang, K., Yang, X., Jiao, L. and Zhang, J. (2024a) 'Rectifying discrepancies between GB-SAR images and terrain model caused by measurement deviations in open-pit mines', *Journal of Circuits, Systems and Computers*, Vol. 33, pp.1–38.

Zheng, X., Haseeb, M., Tahir, Z., Tariq, A., Purohit, S., Soufan, W., Almutairi, K. and Jilani, S.F. (2024b) 'Coupling remote sensing insights with vegetation dynamics and to analyze no 2 concentrations: a Google earth engine-driven investigation', *IEEE Journal of Selected Topics in Applied Earth Observations and Remote Sensing*, Vol. 17, pp.9858–9875.

Zheng, X., Huang, X., Ji, C., Yang, X., Sha, P. and Cheng, L. (2024c) 'Multi-modal person re-identification based on transformer relational regularization', *Information Fusion*, Vol. 103, p.102128.

Zheng, X., Yang, X., Zhao, Q., Zhang, H., He, X., Zhang, J. and Zhang, X. (2024d) 'CFA-GAN: cross fusion attention and frequency loss for image style transfer', *Displays*, Vol. 81, p.102588.